Journal of Pathology
J Pathol 2018; **246:** 67–76
Published online 31 July 2018 in Wiley Online Library (wileyonlinelibrary.com) DOI: 10.1002/path.5110

ORIGINAL PAPER

Genetic instability and recurrent *MYC* amplification in *ALK*-translocated NSCLC: a central role of *TP53* mutations

Christina Alidousty[1], Till Baar[2], Luciano G Martelotto[3], Carina Heydt[1], Svenja Wagener[1], Jana Fassunke[1], Nicolai Duerbaum[1], Andreas H Scheel[1], Sandra Frank[1], Barbara Holz[1], Elke Binot[1], Anna Kron[4], Sabine Merkelbach-Bruse[1], Michaela A Ihle[1], Jürgen Wolf[4,5,6], Reinhard Buettner[1,4,5] and Anne Maria Schultheis[1]*

[1] *University Hospital Cologne, Institute of Pathology, Cologne, Germany*
[2] *University of Cologne, Faculty of Medicine, Institute of Medical Statistics and Computational Biology, Cologne, Germany*
[3] *Monash University, Monash Health, Clayton, Victoria, Australia*
[4] *Network Genomic Medicine, Cologne, Germany*
[5] *Lung Cancer Group Cologne, Department I for Internal Medicine, University Hospital of Cologne, Cologne, Germany*
[6] *Center for Integrated Oncology Cologne Bonn, Germany*

**Correspondence to: Anne Maria Schultheis, Kerpener Straße 62, 50937 Cologne, Germany. E-mail: anne.schultheis@uk-koeln.de*

Abstract

The anaplastic lymphoma kinase (*ALK*) rearrangement defines a distinct molecular subtype of non-small cell lung cancer (NSCLC). Despite the excellent initial efficacy of ALK inhibitors in patients with *ALK*+ lung cancer, resistance occurs almost inevitably. To date, there is no reliable biomarker allowing the identification of patients at higher risk of relapse. Here, we analysed a subset of 53 *ALK*+ tumors with and without *TP53* mutation and *ALK*+ NSCLC cell lines by NanoString nCounter technology. We found that the co-occurrence of early *TP53* mutations in *ALK*+ NSCLC can lead to chromosomal instability: 24% of *TP53*-mutated patients showed amplifications of known cancer genes such as *MYC* (14%), *CCND1* (10%), *TERT* (5%), *BIRC2* (5%), *ORAOV1* (5%), and *YAP1* (5%). MYC-overexpressing *ALK*+ *TP53*-mutated cells had a proliferative advantage compared to wild-type cells. ChIP-Seq data revealed MYC-binding sites within the promoter region of *EML4*, and MYC overexpression in *ALK*+ *TP53*-mutated cells resulted in an upregulation of EML4–ALK, indicating a potential MYC-dependent resistance mechanism in patients with increased *MYC* copy number. Our study reveals that *ALK*+ NSCLC represents a more heterogeneous subgroup of tumors than initially thought, and that *TP53* mutations in that particular cancer type define a subset of tumors that harbour chromosomal instability, leading to the co-occurrence of pathogenic aberrations.

Keywords: *TP53*; chromosomal instability; *ALK*+ adenocarcinoma; lung cancer

Received 19 February 2018; Revised 30 April 2018; Accepted 5 June 2018

No conflicts of interest were declared.

Introduction

Lung cancer is the leading cause of cancer-related deaths worldwide, with about 1.8 million people diagnosed per year [1]. Eighty to 85 per cent of cases belong to the non-small cell lung cancer (NSCLC) group [2]. This term, however, comprises an extremely heterogeneous set of diseases at the molecular level that needs to be translated into therapeutic decision-making [3]. In this context, the anaplastic lymphoma kinase (*ALK*) rearrangement defines a molecular subtype of NSCLC, which is found in the adenocarcinoma histological subtype, predominantly in younger patients and light- or never-smokers [4]. *ALK*, encoding a receptor tyrosine kinase, commonly fuses with *EML4* (echinoderm microtubule-associated protein-like 4) [5], typically resulting in the constitutive activation of the kinase domain, leading to increased pathogenicity via the aberrant activation of downstream signalling pathways.

A recent phase III trial showed that the second-generation ALK inhibitor alectinib outperformed the first approved ALK inhibitor crizotinib, and was associated with longer progression-free survival, lower toxicity, and, in contrast to crizotinib, activity against CNS disease in *ALK*+ NSCLC patients [6]. However, resistance, typically arising within 1–2 years after the first treatment, remains a major concern.

Most NSCLC patients are diagnosed at a late stage of disease, when surgical resection is not performed and diagnoses are made on small biopsy specimens, making comprehensive genomic analyses difficult. To date, the largest series of repeat biopsies from patients with ALK inhibitor-resistant *ALK*+ NSCLC, using a combination of genetic sequencing, histological analyses,

and functional drug screens, was published in 2013 [4]. Despite current knowledge on mechanisms of resistance in NSCLC, there is at present no reliable biomarker allowing the identification of patients at higher risk of relapse.

TP53 is the most frequently mutated gene in human cancers, with about 50% of all tumors harbouring pathogenic mutations within it [7]. One of the main functions of the corresponding protein p53 is to secure genomic stability [8]. In particular, tumors harbouring early pathogenic *TP53* mutations often show high levels of chromosomal instability. High-grade serous ovarian cancer (HGSOC) and serous endometrial carcinomas (ECs), for example, are characterised by extremely high frequencies of *TP53* mutations (96% and 53–90%, respectively) [9] and consequently show high levels of chromosomal instability. In both HGSOC and serous EC, *TP53* mutations are early genetic events, underlining the great importance of mutated *TP53* as a contributor to the tumorigenesis of these chromosomally unstable cancers [10]. Recent clinical data clearly showed that concurrent *TP53* mutations were associated with poorer survival among *ALK*+ NSCLC patients [11].

Here, we hypothesized that early *TP53* mutations in *ALK*+ NSCLC may lead to genetic instability, in particular at the chromosomal level, and that the co-occurrence of *TP53* mutations in *ALK*+ tumors may define a specific subtype of *ALK*+ NSCLCs.

Materials and methods

Patient information and histopathological classification

A total of 423 patients with *ALK*-translocated adenocarcinomas of the lung with sufficient material for molecular diagnostics were included in the study and screened for further clinically targetable genetic alterations as part of the routine molecular diagnostics programme [12] of the Network Genomic Medicine (Cologne, Germany) between January 2011 and December 2017. Comprehensive genomic work-up was available for 147 of 423 patients only. All primary diagnoses were made in accordance with the current WHO (World Health Organisation) classification [13]. Prior to the study, patients had signed written informed consent. The study was conducted in concordance with local ethical guidelines and was reviewed and approved by the institutional ethics committee.

DNA extraction

All tumor samples were formalin-fixed and paraffin-embedded (FFPE) according to local practice. Three to nine 10-µm sections were cut from FFPE tissue blocks. Tumor areas were macrodissected from unstained slides using a marked haematoxylin and eosin (H&E)-stained slide as reference. After deparaffinisation and proteinase K digestion, the DNA was isolated with the Maxwell® 16 FFPE Plus Tissue LEV DNA Purification Kit (Promega, Mannheim, Germany) on the Maxwell® 16 (Promega) following the manufacturer's instructions.

Targeted massively parallel sequencing

For next-generation sequencing (NGS), the DNA content was measured using a quantitative real-time PCR (qPCR) kit (GoTaq qPCR Master Mix; Promega). Multiplex PCR-based parallel sequencing was performed on all FFPE samples. Isolated DNA was amplified with a customised GeneRead DNAseq Targeted Panel V2 (Qiagen, Hilden, Germany) and the GeneRead DNAseq Panel PCR Kit V2 (Qiagen) or an Ion AmpliSeq Custom DNA Panel (Thermo Fisher Scientific, Waltham, MA, USA) and the Ion AmpliSeq Library Kit 2.0 (Thermo Fisher Scientific), following the manufacturer's instructions. Analysed genes and corresponding panels are listed in the supplementary material, Tables S1–S3.

Libraries were constructed using the Gene Read DNA Library I Core Kit and the Gene Read DNA I Amp Kit (Qiagen). After end-repair and adenylation, NEXTflex DNA Barcodes were ligated (Bio Scientific, Austin, TX, USA). Barcoded libraries were amplified, and final library products were quantified, diluted, and pooled in equal amounts. Finally, 12 pmol of the constructed libraries was sequenced on the MiSeq (Illumina, San Diego, CA, USA) with a MiSeq reagent kit V2 (300 cycles) (Illumina) following the manufacturer's recommendations.

Data were exported as FASTQ files. Alignment and annotation were done using a modified version of a previously described method [14]. BAM files were visualised in the Integrative Genomics Viewer (http://www.broadinstitute.org/igv/, Cambridge, MA, USA). A 5% cut-off for variant calls was used and results were only interpreted if the coverage was greater than 200.

Fluorescence *in situ* hybridisation (FISH) analysis

FISH analyses were performed as previously described [15,16] with a few modifications: 2-µm-thick tissue sections were mounted on silanised slides and hybridised overnight with the respective probes according to the manufacturer's instructions (ZytoVision, Bremerhaven, Germany). For *ALK* FISH analysis, the ZytoLight® SPEC ALK/EML4 TriCheck™ (ZytoVision) probe was used. One hundred tumor cell nuclei were counted per case, and break apart or extra red signals were classified as aberrant. A cut-off value of 15% aberrant signals was used to validate the *ALK* translocation as described previously [12,16]. For *MYC* FISH analyses, hybridisation was performed with a ZytoLight® SPEC *MYC*/CEN 8 Dual Color Probe (ZytoVision). For *MYC* amplification, a ratio of MYC/CEN ≥ 2 or an average of ≥6 MYC signals per cell was used.

Immunohistochemistry (IHC)

IHC was performed on FFPE samples to analyse the protein expression of p53. The staining was performed with the BOND-MAX automated immunohistochemistry slide staining system (Leica). The following antibody and conditions were applied: p53 clone DO7 mouse monoclonal (Dako; FFPE retrieving conditions: 20 min in citrate buffer, pH 6; dilution: 1:800; incubation: 20 min, 100 °C).

NanoString nCounter assay

Of the 147 patients with comprehensive clinical follow-up data (described above), only 53 FFPE samples with sufficient material for further NanoString analysis were available (21 with *TP53* mutation and 32 with wild-type *TP53*, both groups exclusively selected based on DNA availability) and analysed using the NanoString nCounter platform (NanoString Technologies, Seattle, WA, USA). Copy number analysis was performed as previously described [17] using 200–600 ng of genomic DNA extracted as described above.

Cell culture and growth assays

The human *ALK*+ NSCLC cell line H3122 was kindly provided by Professor Martin Sos (University of Cologne, Institute of Pathology). A549$^{EML4-ALK}$ and H2228 cell lines were purchased from ATCC (*EML4–ALK* Fusion-A549 Isogenic Cell Line Human, ATCC® CCL185IG™ and NCI-H2228, ATCC® CRL5935™). *ALK* rearrangement was confirmed in all three cell lines by FISH analysis, and *TP53* status, as well as the presence of other known NSCLC typical mutations of the cells, was confirmed by NGS as described above. All cell lines were tested regularly for mycoplasma contamination by means of PCR using the following primers: forward: GGGAGCAAACAGGATTAGATACCCT; reverse: TGCACCATCTGTCACTCTGTTAACCTC. Cells were cultured in RPMI 1640 supplemented with 10% FCS, 100 units/ml penicillin, and 100 µg/ml streptomycin. Cells were maintained in humidified air with 5% CO_2 at 37 °C.

Cell proliferation was measured using the ATPlite Luminescence Assay Kit (Perkin Elmer, Waltham, MA, USA) according to the manufacturer's instructions. In brief, 500 cells were seeded in 100 µl of RPMI medium in 96-well plates 24 h post-transfection with pcDNA3 control plasmid or pcDNA3-cMYC expressing vector. Luminescence was measured after 24 h by means of a Centro LB 960 microplate Luminometer (Berthold Technologies, Bad Wildbach, Germany).

Transient transfections

H3122 and H2228 cells were transfected with the lipid-based transfection reagent Lipofectamine® 3000 (Thermo Fisher Scientific), and A549$^{EML4-ALK}$ cells were transfected with FuGENE® HD Transfection Reagent (Promega, Mannheim, Germany) according to the manufacturer's protocols. pcDNA3-cMYC plasmid was a gift from Wafik El-Deiry (Addgene plasmid # 16011) [18].

Preparation of whole cell lysates and immunoblotting

Cells were harvested, washed once with ice-cold PBS, and lysed with 1 ml of RIPA buffer (Sigma-Aldrich, St Louis, MO, USA) containing protease inhibitors (complete mini, Roche Diagnostics GmbH, Mannheim, Germany). After 15 min on ice, lysates were centrifuged (15 min, 4 °C, 14 000 rpm) and supernatants were collected and stored at −80 °C until 50–100 µg of lysates was subjected to SDS-polyacrylamide gel electrophoresis. Protein concentrations were determined by means of a Qubit™ Protein Assay Kit (Invitrogen, Carlsbad, CA, USA), according to the manufacturer's instructions. Proteins were transferred to a nitrocellulose membrane and detected using Lumi-Light/Lumi Light^{PLUS} Western blotting Substrate (Roche Applied Science, Penzberg, Germany) with MYC antibody [polyclonal anti-c-MYC antibody (ab86356); Abcam, Cambridge, UK]. To ensure equal protein loading of the cell lysates, blots were incubated with a monoclonal GAPDH-specific antibody (Novus Biologicals, Littleton, CO, USA).

RNA extraction and quantitative real-time PCR

Total RNA was purified using a my-Budget RNA Mini Kit (Bio-Budget, Krefeld, Germany) according to the manufacturer's protocol. First-strand cDNA was synthesised with an ImProm-II™ Reverse Transcription System (Promega, Mannheim, Germany). Real-time PCR was carried out on the Light Cycler Instrument II (Roche, Basel, Switzerland). TaqMan master mix and TaqMan primer sets were obtained for human MYC (Hs00153408_m1), human EML4–ALK (Hs04419883_ft), and human GAPDH (Hs03929097_g1) as an internal control (Thermo Fisher Scientific). Results were calculated using the comparative deltaCT methodology.

ChIP-Seq

ChIP-Seq was performed through Active Motif Epigenetic Services according to their procedures. Reads were aligned to the human genome (hg19) using the BWA algorithm (default settings) [19].

Bioinformatic and statistical analyses

Copy number plots

The read count data obtained from the NanoString analyses were plotted using the ggPlot2 package v2.2.1 [20] for R v3.4.0 [21], expanded with the ggthemes package v3.4.0 [22]. Data processing was accomplished using the plyr v1.8.4 [23], dplyr v.0.7.0 [24], reshape2 v1.4.2 [25], and stringr v1.2.0 [26] packages. For each sample, the counts were plotted according to their position in

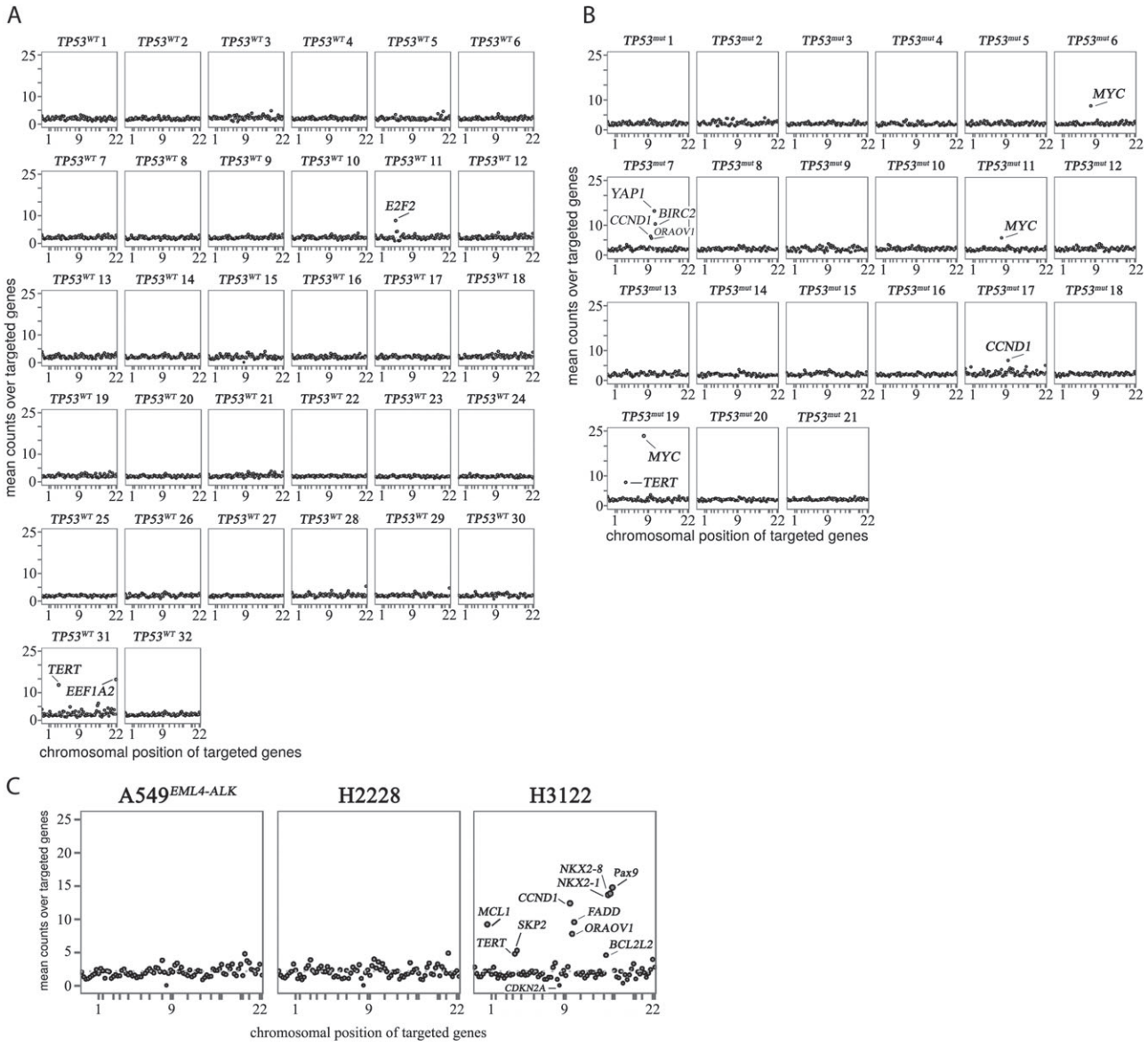

Figure 1. *TP53* deficiency causes genomic instability in *ALK*+ lung tumors. Copy number plots of *ALK*+ samples from patients without (A) or with (B) *TP53* mutation or cell lines harbouring wild-type (C, left and middle plot) or mutated *TP53* (C, right plot). The copy numbers of 87 genes were determined by means of NanoString nCounter technology. Absolute copy numbers (*Y*-axis) for each gene are plotted according to their chromosomal location (*X*-axis).

the genome and their magnitude. Both axes are linearly scaled and equal for all displayed plots.

Clonality analysis

Clonality analysis was performed as previously described [27]. The code provided by Youn and Simon (written in R) was executed with standard parameters, using 200 bootstrap replicates on a 25 × 14 data matrix (samples × genes). By this method, the relative mutation order probability distribution during tumorigenesis was estimated from genome sequencing data. As the available tumor samples were analysed using amplicon-based sequencing with several different multiplex primer panels, only the largest group of consistently sequenced samples was used for estimation. This reduced the sample size to 25 (57%) individual tumors.

Brown–Forsythe test

To assess whether samples harbouring a *TP53* mutation showed a statistically significant higher chromosomal instability, a Brown–Forsythe test was performed [28]. Any result of a given locus differing from the expected value of $n = 2$ gene copies was defined as a genetic event.

Results

To investigate whether *TP53* mutations in *ALK*+ tumors cause genetic instability, we analysed a subset of 53 *ALK*+ tumors, 21 harbouring a pathogenic *TP53* mutation and 32 with wild-type *TP53*, as well as three *ALK*+ cell lines, with (H3122) or without (A549$^{EML4-ALK}$, H2228) *TP53* mutation, regarding changes in the copy

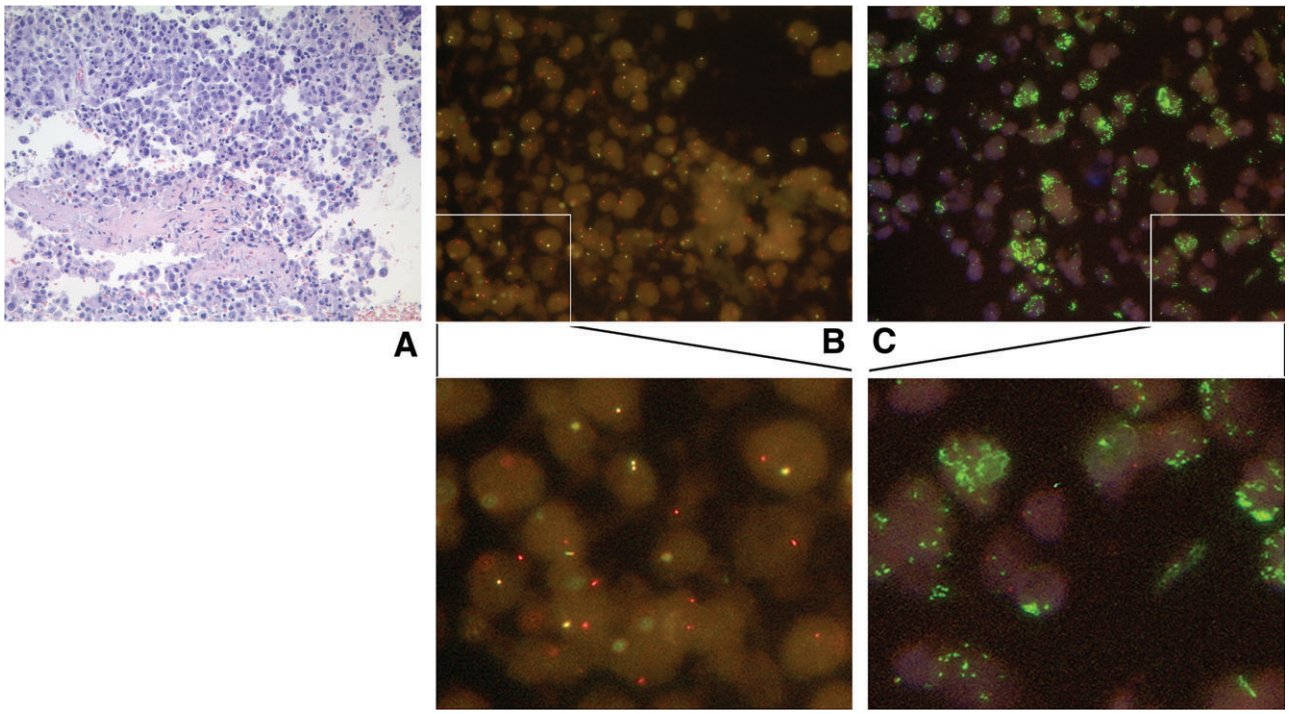

Figure 2. Histology of ALK+/*TP53*^{mut} lung-adenocarcinoma-tumor tissue (patient *TP53*^{mut} 19). (A) Representative H&E-stained tumor. (B) FISH analysis showing *ALK* rearrangement. Yellow signals represent an intact *ALK* gene, while separated red and green or isolated red signals represent a split-apart *ALK* gene. The probes used are described in ref 16. (C) FISH analysis showing *MYC* amplification. Green signals represent *MYC*; red signals represent the control locus *D8Z2* (chr. 8 centromere). The images were taken at 60× magnification.

number of 87 cancer-relevant genes. The particular type of *TP53* mutation and/or the corresponding p53 immunohistochemical staining pattern were determined for each patient with sufficient available material (supplementary material, Tables S4 and S5). The staining patterns correlated with the respective type of mutation found by NGS and examples of the three possible p53 staining patterns are shown in the supplementary material, Figure S1. In all three cell lines, as well as in most tumor samples, *ALK* was fused to its most common fusion partner, *EML4*, and translocation occurred in a high percentage of tumor cells (supplementary material, Tables S4 and S5). No further *ALK+/TP53*^{mut} cell lines were commercially available, limiting the number of cell lines analysed to one (*TP53*^{WT}) or two (*TP53*^{mut}), respectively.

As shown in Figure 1A, *ALK+/TP53*^{WT} samples displayed mostly chromosomally stable genomic profiles in terms of copy number alterations, with a few exceptions: patient *TP53*^{WT} 11 had eight copies of *E2F3*, and patient *TP53*^{WT} 31 showed 13 copies of *TERT* and 15 copies of *EEF1A2*.

In contrast, the total number of genomic events in *ALK+/TP53*^{mut} samples was elevated (Figure 1B). Strikingly, a recurrent *MYC* gene amplification was found in 3 of the 21 cases. The *MYC* copy numbers were 8 (patient *TP53*^{mut} 6), 6 (patient *TP53*^{mut} 11), and 23 (patient *TP53*^{mut} 19). In all cases, *ALK* rearrangement and *TP53* mutations were determined prior to therapy. To compare differences in gene amplifications before and after treatment, one patient (*TP53*^{mut} 11) was analysed before (primary tumor) and after (local recurrence) crizotinib administration: no remarkable differences between these samples could be found (supplementary material, Figure S2). For all analysed cases, *ALK* rearrangement and, if present, *MYC* amplifications were validated using FISH as depicted in the representative histology image (Figure 2). Biallelic *TP53* deletions, which could potentially cause chromosomal instability, did not occur in the analysed cohort (*TP53* copy number > 0 in all analysed cases).

To determine whether the number of copy number alterations differed significantly between *ALK+/TP53*^{WT} and *ALK+/TP53*^{mut} samples, a Brown–Forsythe statistical test was performed. The resulting P value applied to the NanoString count data of both groups was $p = 2.24 \times 10^{-4}$, lying far below the significance threshold of $p = 0.05$. Consequently, both groups were considered to be heteroscedastic (possessing statistically significant differences in their group variances). The actual variance values were 0.52 for *ALK+/TP53*^{WT} and 0.87 for *ALK+/TP53*^{mut}, showing that *ALK+/TP53*^{mut} cases possess a higher variance and consequently an elevated number of events in terms of changes in gene copy number.

To further validate the finding that *ALK+/TP53*^{mut} tumors harbour chromosomal instability, we analysed the three *ALK*+ cell lines harbouring either *TP53*^{WT} (A549$^{EML4-ALK}$, H2228) or *TP53*^{mut} (H3122) regarding differences in the respective copy numbers. The NanoString analysis revealed findings consistent with the analysis of patient samples: the *ALK+/TP53*^{WT} cells

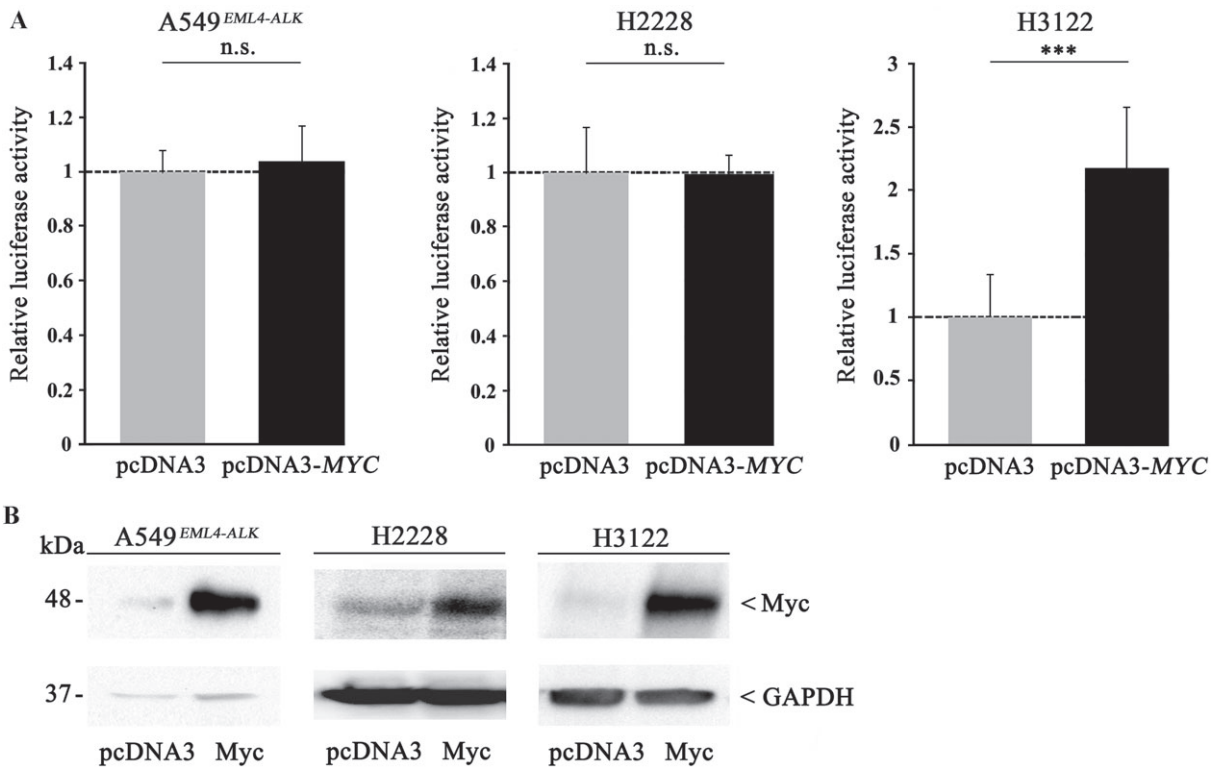

Figure 3. MYC enhances cell proliferation only in *TP53*^{mut} but not in *TP53*^{WT} *ALK*+ cell lines. (A) A549$^{EML4-ALK}$ (left), H2228 (middle), and H3122 (right) were transiently transfected with a pcDNA3-*MYC* expression plasmid or pcDNA3 vector as control. Twenty-four hours after transfection, cells were seeded in 96-well plates and luminescence was measured after 24 h by means of a Centro LB 960 microplate luminometer. Each experiment was performed independently and at least in triplicates, and each measurement was carried out with eight technical replicates. All values are expressed as means ±standard deviation. Statistical significance was evaluated using Student's *t*-test: n.s. = not significant, $p > 0.05$; ***$p \leq 0.001$. (B) MYC overexpression was confirmed by immunoblot analysis in A549$^{EML4-ALK}$ (left), H2228 (middle), and H3122 (right) using a polyclonal anti-MYC antibody. Equal protein loading was ensured by determining GAPDH levels.

had relatively stable genomes and gene copy numbers did not exceed $n = 5$. In contrast, the amount of CNA in H3122 cells was increased (Figure 1C, right), with seven gene loci showing copy numbers in the range of 6–15.

Given the fact that *ALK* rearrangements are dominant oncogenic drivers, making the accumulation of further mutations redundant, we wanted to investigate if *TP53* mutations occur early during tumorigenesis, leading to genomic instability. We performed a clonality analysis approach, analysing different gene mutations with respect to the time of occurrence in the process of tumor formation (supplementary material, Figure S3) [27]. Despite the reduced sample size (see the Materials and methods section), the *TP53* mutation in all analysed tumors was estimated to be an early genetic event (i.e. one of the first three mutations to occur) with a probability of 89%, given a 90% confidence interval ranging from 68% to 100%.

The fact that around 14% of the patients with co-occurrence of *TP53* mutation and *ALK* rearrangement showed simultaneous amplifications of *MYC*, together with the observation that two of these three patients progressed on therapy within less than 1 year (with none of the common resistance mechanisms, namely *KRAS*, *EGFR*, *ALK* mutations and *EGFR*, *MET*, *HER2* and *ALK* amplifications), prompted us to investigate further the relationship between *MYC* and *TP53* in the given context. As patient *TP53*^{mut} 19 was diagnosed recently, no clinical follow-up data were available, making the prediction of disease progression impossible. Currently, the treating physicians are being contacted to collect further comprehensive clinical data on all analysed cases. At the time of this study, only clinical data from the pathology charts could be accessed.

To further evaluate the role of *MYC* in *ALK*+ tumors, we transiently overexpressed MYC in A549$^{EML4-ALK}$, H2228 (both *TP53*^{WT}), and H3122 cells (*TP53*^{mut}), and measured the proliferation rate in all three cell lines. As shown in Figure 3A, H3122 cells with elevated MYC content showed a two-fold increase in the proliferation rate compared with cells transfected with control vector. In contrast, there was no difference in cell growth in *TP53*^{WT} A549$^{EML4-ALK}$ or H2228 cells with increased MYC levels. Overexpression of MYC protein was confirmed in all cell lines by western blot analysis (Figure 3B).

In order to further understand the underlying mechanisms of MYC-induced cell proliferation, we performed ChIP-Seq (chromatin immunoprecipitation DNA sequencing) analyses and found MYC-binding sites within the EML4-promoter region (Figure 4A), suspecting possible MYC-induced expression of EML4–ALK. Given the fact that we found *MYC* amplifications in

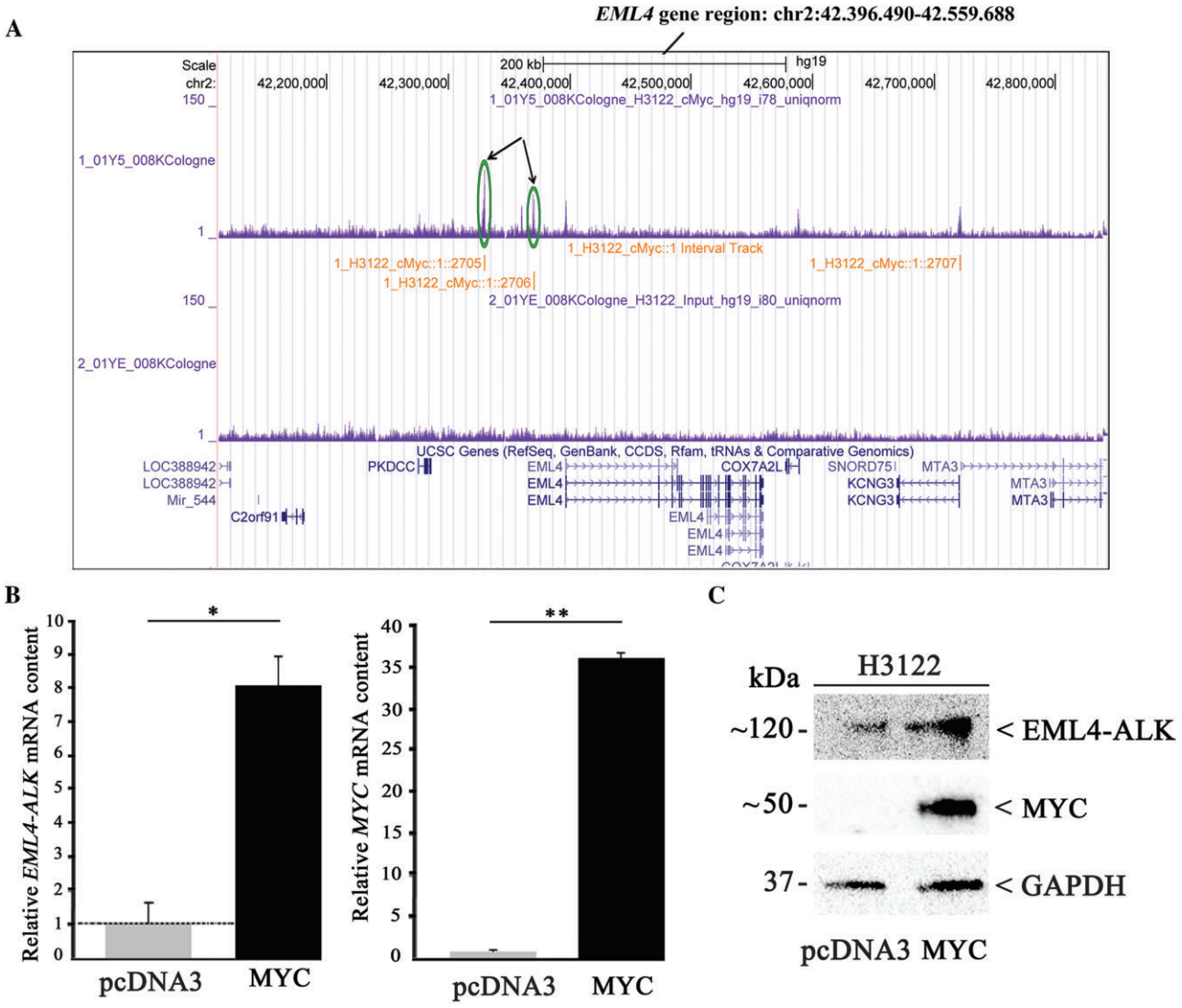

Figure 4. MYC upregulates EML4–ALK expression in *TP53*-mutated H3122 cells. H3122 cells were transiently transfected with a MYC expression plasmid or pcDNA3 vector as control. (A) ChIP-Seq analyses revealed MYC binding sites within the *EML4–ALK* promoter region (green circles and arrows). (B) *MYC* and *EML4–ALK* mRNA levels were determined by TaqMan gene expression assay. The values shown were normalised to control transfection. All values are expressed as means ±standard deviation. Statistical significance was evaluated using the Student's *t*-test: $^{*}p \leq 0.05$, $^{**}p \leq 0.01$. (C) EML4–ALK and MYC protein amounts were determined by immunoblot analysis using a monoclonal anti-ALK or a polyclonal anti-MYC antibody. Equal protein loading was ensured by determining GAPDH levels.

TP53^{mut} *ALK*+ patients exclusively, experiments were performed with the only available *ALK*+/*TP53*^{mut} cell line, H3122. Overexpression of MYC in H3122 cells resulted in an increased EML4–ALK content, both at the RNA (Figure 4B, left) and protein (Figure 4C) levels.

Discussion

Drug resistance in *ALK*+ NSCLC patients continues to be a major impediment. In recent years, the analyses of post-treatment tumor tissue samples have massively improved our understanding of the molecular mechanisms of resistance to ALK inhibitors: Camidge *et al* [29] were the first to divide mechanisms of resistance to ALK inhibitors (i.e. crizotinib) into two types: ALK dominant (on-target) and ALK non-dominant (off-target). The ALK-dominant type, representing approximately 50% of cases, is characterised by secondary mutations of the ALK kinase domain or copy number gains of the *ALK* gene (*ALK* amplifications), whereas the non-dominant type includes the activation of alternative oncogenic pathways (e.g. EGFR, KRAS, KIT, MET, IGF1R pathways), which may cause resistance independently of *ALK* genetic alterations. *EGFR* and *KRAS* mutations [30], amplification of *KIT* [31] or activation of the IGF1R pathway [32] are possible resistance mechanisms leading to insensitivity to crizotinib. Other mechanisms of resistance include epithelial–mesenchymal transition (EMT) [33] and autophagy [34].

A recent study showed that 33% of *ALK*+ tumors exhibit mutations within *TP53*, whereby it could not be

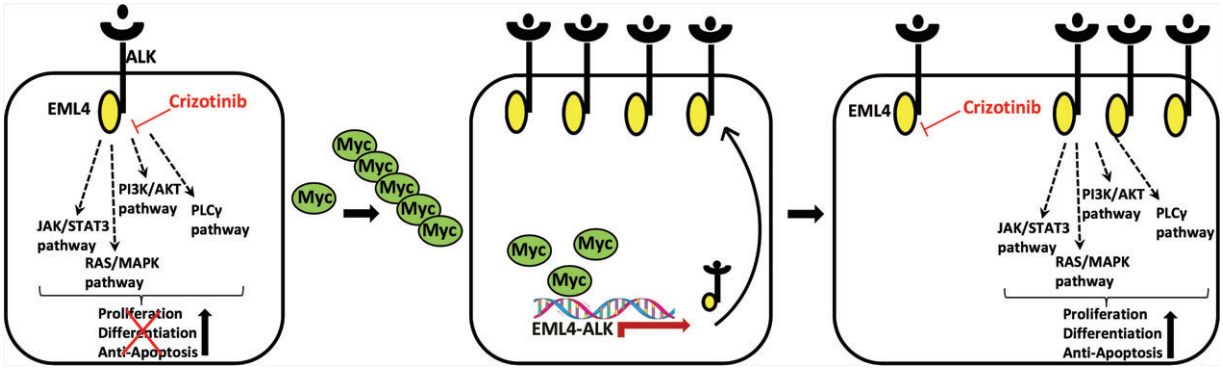

Figure 5. Proposed mechanism for MYC-dependent resistance to ALK inhibitors in *TP53*-mutated *ALK*+ NSCLC patients. ALK inhibitors such as crizotinib block EML4–ALK-mediated proliferation of cancer cells (left). *MYC* amplification leads to enhanced binding of the oncogene to the *EML4–ALK* promoter, resulting in increased expression of the kinase (middle), causing resistance to crizotinib (right).

determined whether these mutations were present prior to treatment with second-generation ALK inhibitors or were a result of the therapy [35]. In our institution, we observed that 23.8% of all *ALK*+ cases harboured an additional *TP53* mutation prior to treatment. In this context, we wanted to further investigate the impact of *TP53* mutations in this particular tumor type. Our analyses revealed that *TP53* mutations occur early during tumorigenesis, which is in line with the observed genomic instability in these *ALK*+ tumors. Aisner *et al* recently showed that concurrent *TP53* mutations are associated with poorer survival among *ALK*+ NSCLC patients [11]. They suggested that *TP53* mutations lead to genetic instability in lung adenocarcinoma and thus may accelerate the development of multiple mechanisms of resistance to targeted therapy in these patients, resulting in shorter survival. The relationship between chromosomal instability caused by early mutations in *TP53* and the exact underlying molecular mechanisms of resistance still need to be elucidated.

Seo *et al* did not find any *MYC* copy number changes in ten patients with *ALK*+ lung adenocarcinoma [36]. In contrast, we have shown that 14% of *ALK*+/*TP53*-mutated patients had *MYC* amplification, which was not observed in $TP53^{WT}$ cases. *MYC* is one of the most frequently amplified oncogenes among many different human cancers and is involved in tumorigenesis in these tumors [37].

Our functional experiments using *ALK*+ H3122 ($TP53^{mut}$) and H2228 and A549$^{EML4–ALK}$ (both $TP53^{WT}$) cells revealed a proliferative advantage after MYC overexpression only in the absence of intact *TP53*, suggesting a potential *TP53*-dependent MYC-induced growth advantage. The impact of copy number alterations on therapy resistance has already been proven in different cancer types and it is known that patients with gene amplifications can become resistant to drug therapies, resulting in a poor prognosis [38]. Several studies indicate that MYC overexpression is associated with drug resistance [39,40], leading to the assumption that increased *MYC* copy number might also have a negative impact on *ALK*+ patients' outcome.

By ChIP-Seq, we found MYC binding sites within the *EML4* promoter region, as well as MYC-induced increased levels of EML4–ALK RNA and protein, after overexpression of the oncogene. These preliminary findings let us propose a MYC-induced resistance mechanism in *ALK*+ *TP53*-deficient patients; this could be categorised according to Gainor *et al* [35] as an 'ALK-dominant mechanism': *MYC* amplification and overexpression lead to increased binding of the oncogene to the EML4–ALK promoter, thereby increasing the expression of EML–ALK within the cells and causing resistance to ALK inhibitors (Figure 5). Several studies have reported that changes in *MYC* copy number are associated with aggressive behaviour in different cancer types, and it is reported that c-MYC and n-MYC, another member of the MYC oncoprotein family, are downstream targets of ALK signalling in *ALK*+ anaplastic large cell lymphomas [41,42], suggesting a positive feedback loop in the MYC/EML4–ALK axis. MYC appears to be a universal amplifier of gene expression, increasing output at all active promoters in tumor cells [43], which is in line with our results.

Compared with *TP53*-deficient patients, $ALK+/TP53^{WT}$ patients had genetically stable genomes, with one noteworthy exception: patient $TP53^{WT}$ 31 showed a genomic-unstable DNA profile, with amplification of diverse genes, including *EEF1A2* (15 copies) and *TERT* (13 copies). In cancer cells, telomere dysfunction leads to genomic instability [44]. By activation of telomerase, telomere function is reconstituted, resulting in highly proliferative, immortalised telomerase-positive cells with heavily rearranged genomes [45]. The genomic instability in patient $TP53^{WT}$ 31 may be explained by TERT reconstitution caused by the amplification of the corresponding gene. Analyses of larger numbers of cases will be required to confirm these observations.

Acknowledgements

The research reported in this article was funded by Roche Pharma AG and the Kölner Krebsstiftung. We

thank Christian Reinboth for his excellent assistance with the immunohistochemical p53 staining.

Author contributions statement

AMS, CA, LGM, and RB conceived the study. CA, BH, EB, SW, ND, SF, CH, SMB, JF, and MAI performed experiments and analysed the data. TB performed bioinformatics analysis. AMS, RB, and CA discussed and interpreted the results. CA, AMS, RB, SMB, JW, AK, and AHS wrote/reviewed the manuscript. All of the authors read, edited, and approved the final manuscript.

References

1. Torre LA, Bray F, Siegel RL, *et al.* Global cancer statistics, 2012. *CA Cancer J Clin* 2015; **65:** 87–108.
2. Reck M, Popat S, Reinmuth N, *et al.* Metastatic non-small-cell lung cancer (NSCLC): ESMO Clinical Practice Guidelines for diagnosis, treatment and follow-up. *Ann Oncol* 2014; **25**(suppl 3): iii27–39.
3. Boolell V, Alamgeer M, Watkins DN, *et al.* The evolution of therapies in non-small cell lung cancer. *Cancers (Basel)* 2015; **7:** 1815–1846.
4. Gainor JF, Varghese AM, Ou SH, *et al.* ALK rearrangements are mutually exclusive with mutations in *EGFR* or *KRAS*: an analysis of 1,683 patients with non-small cell lung cancer. *Clin Cancer Res* 2013; **19:** 4273–4281.
5. Soda M, Choi YL, Enomoto M, *et al.* Identification of the transforming *EML4–ALK* fusion gene in non-small-cell lung cancer. *Nature* 2007; **448:** 561–566.
6. Peters S, Camidge DR, Shaw AT, *et al.* Alectinib versus crizotinib in untreated ALK-positive non-small-cell lung cancer. *N Engl J Med* 2017; **377:** 829–838.
7. Vogelstein B, Lane D, Levine AJ. Surfing the p53 network. *Nature* 2000; **408:** 307–310.
8. Chumakov PM. Versatile functions of p53 protein in multicellular organisms. *Biochemistry (Mosc)* 2007; **72:** 1399–1421.
9. Lax SF, Kendall B, Tashiro H, *et al.* The frequency of p53, K-*ras* mutations, and microsatellite instability differs in uterine endometrioid and serous carcinoma: evidence of distinct molecular genetic pathways. *Cancer* 2000; **88:** 814–824.
10. O'Hara AJ, Bell DW. The genomics and genetics of endometrial cancer. *Adv Genomics Genet* 2012; **2012:** 33–47.
11. Aisner DL, Sholl LM, Berry L, *et al.* The impact of smoking and TP53 mutations in lung adenocarcinoma patients with targetable mutations – the Lung Cancer Mutation Consortium (LCMC2). *Clin Cancer Res* 2018; **24:** 1038–1047.
12. Heydt C, Kostenko A, Merkelbach-Bruse S, *et al.* ALK evaluation in the world of multiplex testing: Network Genomic Medicine (NGM): the Cologne model for implementing personalised oncology. *Ann Oncol* 2016; **27**(suppl 3): iii25–iii34.
13. Travis WD, Brambilla E, Burke AP, *et al* (eds). *WHO Classification of Tumours of the Lung, Pleura, Thymus and Heart* (4th edn). International Agency for Research on Cancer: Lyon, 2015.
14. Peifer M, Fernandez-Cuesta L, Sos ML, *et al.* Integrative genome analyses identify key somatic driver mutations of small-cell lung cancer. *Nat Genet* 2012; **44:** 1104–1110.
15. Schultheis AM, Bos M, Schmitz K, *et al.* Fibroblast growth factor receptor 1 (FGFR1) amplification is a potential therapeutic target in small-cell lung cancer. *Mod Pathol* 2014; **27:** 214–221.
16. Schildhaus HU, Deml KF, Schmitz K, *et al.* Chromogenic *in situ* hybridization is a reliable assay for detection of ALK rearrangements in adenocarcinomas of the lung. *Mod Pathol* 2013; **26:** 1468–1477.
17. Kim ST, Lee SJ, Park SH, *et al.* Genomic profiling of metastatic gastroenteropancreatic neuroendocrine tumor (GEP-NET) patients in the personalized-medicine era. *J Cancer* 2016; **7:** 1044–1048.
18. Ricci MS, Jin Z, Dews M, *et al.* Direct repression of FLIP expression by c-myc is a major determinant of TRAIL sensitivity. *Mol Cell Biol* 2004; **24:** 8541–8555.
19. Li H, Durbin R. Fast and accurate short read alignment with Burrows–Wheeler transform. *Bioinformatics* 2009; **25:** 1754–1760.
20. Wickham H. *ggplot2: Elegant Graphics for Data Analysis*. Springer-Verlag: New York, 2009.
21. The R code Team. R: A Language and Environment For Statistical Computing. [Accessed 2017]. Available from: https://www.R-project.org/
22. Arnold JB. ggthemes: Extra Themes, Scales and Geoms for 'ggplot2'. [Accessed 2017]. Available from: https://CRAN.R-project.org/package=ggthemes
23. Wickham H. The split–apply–-combine strategy for data analysis. *J Stat Software* 2011; 1–29; DOI: 10.18637/jss.v040.i01 [Epub ahead of print].
24. Wickham H. dplyr: A Grammar of Data Manipulation. [Accessed 2017]. Available from: https://CRAN.R-project.org/package=dplyr
25. Wickham H. Reshaping data with the reshape package. *J Stat Software* 2007; **21:** DOI: 10.18637/jss.v021.i12.
26. Wickham H. stringr: Simple, Consistent Wrappers for Common String Operations. [Accessed 2017]. Available from: https://CRAN.R-project.org/package=stringr
27. Youn A, Simon R. Estimating the order of mutations during tumorigenesis from tumor genome sequencing data. *Bioinformatics* 2012; **28:** 1555–1561.
28. Brown MB, Forsythe AB. Robust tests for the equality of variances. *J Am Stat Assoc* 1974; **69:** 364–367.
29. Camidge DR, Doebele RC. Treating ALK-positive lung cancer – early successes and future challenges. *Nat Rev Clin Oncol* 2012; **9:** 268–277.
30. Doebele RC, Pilling AB, Aisner DL, *et al.* Mechanisms of resistance to crizotinib in patients with ALK gene rearranged non-small cell lung cancer. *Clin Cancer Res* 2012; **18:** 1472–1482.
31. Katayama R, Shaw AT, Khan TM, *et al.* Mechanisms of acquired crizotinib resistance in ALK-rearranged lung cancers. *Sci Transl Med* 2012; **4:** 120ra17.
32. Lovly CM, McDonald NT, Chen H, *et al.* Rationale for co-targeting IGF-1R and ALK in ALK fusion-positive lung cancer. *Nat Med* 2014; **20:** 1027–1034.
33. Kim HR, Kim WS, Choi YJ, *et al.* Epithelial–mesenchymal transition leads to crizotinib resistance in H2228 lung cancer cells with EML4–ALK translocation. *Mol Oncol* 2013; **7:** 1093–1102.
34. Ji C, Zhang L, Cheng Y, *et al.* Induction of autophagy contributes to crizotinib resistance in ALK-positive lung cancer. *Cancer Biol Ther* 2014; **15:** 570–577.
35. Gainor JF, Dardaei L, Yoda S, *et al.* Molecular mechanisms of resistance to first- and second-generation ALK inhibitors in ALK-rearranged lung cancer. *Cancer Discov* 2016; **6:** 1118–1133.
36. Seo AN, Yang JM, Kim H, *et al.* Clinicopathologic and prognostic significance of *c-MYC* copy number gain in lung adenocarcinomas. *Br J Cancer* 2014; **110:** 2688–2699.
37. Beroukhim R, Mermel CH, Porter D, *et al.* The landscape of somatic copy-number alteration across human cancers. *Nature* 2010; **463:** 899–905.
38. Bertotti A, Papp E, Jones S, *et al.* The genomic landscape of response to EGFR blockade in colorectal cancer. *Nature* 2015; **526:** 263–267.
39. Walker TL, White JD, Esdale WJ, *et al.* Tumour cells surviving *in vivo* cisplatin chemotherapy display elevated c-*myc* expression. *Br J Cancer* 1996; **73:** 610–614.

40. McNeil CM, Sergio CM, Anderson LR, *et al.* c-Myc overexpression and endocrine resistance in breast cancer. *J Steroid Biochem Mol Biol* 2006; **102:** 147–155.
41. Raetz EA, Perkins SL, Carlson MA, *et al.* The nucleophosmin-anaplastic lymphoma kinase fusion protein induces c-Myc expression in pediatric anaplastic large cell lymphomas. *Am J Pathol* 2002; **161:** 875–883.
42. Gustafson WC, Weiss WA. Myc proteins as therapeutic targets. *Oncogene* 2010; **29:** 1249–1259.
43. Nie Z, Hu G, Wei G, *et al.* c-Myc is a universal amplifier of expressed genes in lymphocytes and embryonic stem cells. *Cell* 2012; **151:** 68–79.
44. Artandi SE, Chang S, Lee SL, *et al.* Telomere dysfunction promotes non-reciprocal translocations and epithelial cancers in mice. *Nature* 2000; **406:** 641–645.
45. Maciejowski J, de Lange T. Telomeres in cancer: tumour suppression and genome instability. *Nat Rev Mol Cell Biol* 2017; **18:** 175–186.

SUPPLEMENTARY MATERIAL ONLINE

Supplementary figure legends

Figure S1. Three immunohistochemical staining patterns of p53 in *ALK*+ patients

Figure S2. Copy number plots of primary tumor and local recurrence of the same *ALK+/TP53*^{mut} patient

Figure S3. *TP53* mutation is an early event during tumorigenesis in *ALK*-driven tumors

Table S1. NGS results from the *EML4–ALK*-translocated cell line H2888

Table S2. NGS results from the *EML4–ALK*-translocated cell line H3122

Table S3. NGS results from the *EML4–ALK*-translocated cell line A549$^{EML4–ALK}$

Table S4. Characteristics of patients (*TP53*^{WT})

Table S5. Characteristics of patients (*TP53*^{mut})